Published in final edited form as:
Biochim Biophys Acta. 2012 May ; 1818(5): 1261–1268. doi:10.1016/j.bbamem.2012.02.008.

NMR Structures of the Transmembrane Domains of the α4β2 nAChR

Vasyl Bondarenko[1], **David Mowrey**[1,3], **Tommy Tillman**[1], **Tanxing Cui**[1,2], **Lu Tian Liu**[1], **Yan Xu**[1,2,4], and **Pei Tang**[1,3,4,*]

[1]Department of Anesthesiology, University of Pittsburgh School of Medicine

[2]Department of Structural Biology, University of Pittsburgh School of Medicine

[3]Department of Computational Biology, University of Pittsburgh School of Medicine

[4]Department of Pharmacology & Chemical Biology, University of Pittsburgh School of Medicine

Abstract

The α4β2 nicotinic acetylcholine receptor (nAChR) is the predominant heteromeric subtype of nAChRs in the brain, which has been implicated in numerous neurological conditions. The structural information specifically for the α4β2 and other neuronal nAChRs is presently limited. In this study, we determined structures of the transmembrane (TM) domains of the α4 and β2 subunits in lauryldimethylamine-oxide (LDAO) micelles using solution NMR spectroscopy. NMR experiments and size exclusion chromatography–multi-angle light scattering (SEC-MALS) analysis demonstrated that the TM domains of α4 and β2 interacted with each other and spontaneously formed pentameric assemblies in the LDAO micelles. The Na^+ flux assay revealed that α4β2 formed Na^+ permeable channels in lipid vesicles. Efflux of Na^+ through the α4β2 channels reduced intra-vesicle Sodium Green™ fluorescence in a time-dependent manner that was not observed in vesicles without incorporating α4β2. The study provides the structural insight into the TM domains of the α4β2 nAChR. It offers a valuable structural framework for rationalizing extensive biochemical data collected previously on the α4β2 nAChR and for designing new therapeutic modulators.

Keywords

nicotinic acetylcholine receptors; nAChR; α4β2; NMR; ion channel structures; cys-loop receptors

1. Introduction

The nicotinic acetylcholine receptor (nAChR) is a member of the Cys-loop superfamily that mediates fast synaptic transmission in the central and peripheral nervous systems. The α4β2 nAChR is the most abundant heteromeric nAChR subtype in the brain [1]. It has been implicated to play roles in Parkinson's disease [2], Alzheimer's disease [3], nicotine addiction [4, 5], and general anesthesia [6–8].

Send all correspondence to: Professor Pei Tang, Ph.D., 2049 Biomedical Science Tower 3, 3501 Fifth Avenue, University of Pittsburgh, Pittsburgh, Pennsylvania 15260, Tel (412) 383-9798, Fax (412) 648-8998, tangp@upmc.edu.

Despite the importance of the α4β2 nAChR in various neurological conditions, experimental structural characterization of the α4β2 nAChR remains sparse [9–11]. Structural understanding of nAChRs has relied heavily on the Cryo-electron microscopy structural model of the muscle type nAChR found in the electric ray *Torpedo marmorata* [12]. The structural model has only a resolution of 4 Å, but shows a pentameric scaffold and extracellular (EC), transmembrane (TM), and intracellular (IC) domains for each of the five subunits. More recently, homologous structures of the bacteria *Gloebacter violaceous* (GLIC) [13, 14] and *Erwinia chrysanthemi* (ELIC) [15] and the *Caenorhabditis elegans* glutamate-gated chloride channel alpha (GluCl) [16] have been determined at resolutions of 2.9 Å, 3.3 Å, and 3.3 Å, respectively. Unlike mammalian Cys-loop receptors, GLIC and ELIC do not contain a large IC domain. Among the EC, TM and IC domains of Cys-loop receptors, the EC domain containing the orthosteric agonist-binding site has the richest structural information, mainly from crystal structures of the acetylcholine binding protein (AChBPs) [17–19], the EC domain of the mouse α1 subunit [20], and the chimera of the α7 nAChR-AChBP [21]. In contrast, the IC domain connecting TM3 and TM4 is the least studied domain. This domain is the least conserved among nAChR subunits and has the least structural data at present. The IC domain is known to modulate interaction with cytoskeleton components as well as channel desensitization [22]. However, it was demonstrated that fully functional channels could be obtained by replacing the IC domain with a short linker found in GLIC [23].

Although structural understanding of the TM domain is not as inadequate as that on the IC domain, more thorough structural characterizations on the TM domain for individual Cys-loop receptors are required in order to satisfy the demands for rational design of therapeutic drugs and for discovery of molecular mechanisms of drug action [24, 25]. The TM domain contains the channel gate. Hence, it is the critical region for controlling the flow of ions across the membrane [26]. Positive and negative allosteric modulators acting at the TM domains of nAChRs [27–29] have been implicated as useful therapeutics for neurological diseases. The TM domain also provides binding sites for general anesthetics. The intravenous anesthetic etomidate binds to the TM domain of the *Torpedo* nAChR [30]. The inhalational anesthetic halothane shows binding to the TM domain both experimentally in the *Torpedo* nAChR [31] and computationally in the α4β2 and α7 nAChRs [32–34]. High-resolution structural information of nAChR TM domains is therefore important both for characterizing mechanisms of action for existing drugs and indentifying plausible binding sites for new drugs.

While the interplay between the EC and TM domains is critical for transducing ligand-binding signals to the channel gate, the intrinsic folding of the TM domain seems to be independent of the existence of the EC domain. Incorporation of the TM2 helix into a lipid environment was found to produce ion specific channels [35, 36]. Furthermore, we have previously demonstrated faithful folding of the TM domain of the β2 subunit in membrane mimetic microclusters formed by the hexafluoroisopropanol and water mixture (1:1) [9]. Thus, it is reasonable and practical to solve structures of the TM domains in the absence of the EC and IC domains.

In the present study, we used lauryldimethylamine-oxide (LDAO) micelles as a membrane mimetic and solved the NMR structures for the TM domains of the α4 and β2 nAChR subunits. We found that the α4 and β2 TM domains form pentameric assemblies in LDAO micelles. When reconstituted into lipid vesicles, the α4β2 assemblies are capable of transporting Na^+ ions. High-resolution structures of the individual α4 and β2 TM domains and the assembled pentameric structural model for the α4β2 nAChR TM domain provide valuable templates for understanding mechanisms of channel function and drug action as well as for rational drug discoveries.

2. Materials and Methods

2.1 Sample Preparations

The method to obtain the α4 and β2 TM domains of the human nAChR was reported previously [9]. Proteins were expressed in *E. coli* Rosetta 2(DE3) pLysS (Novagen) at 15 °C for ~3 days using the Marley protocol [37]. The EC domain at the N-terminus was replaced with a TEV protease recognition site and a histidine tag. A short synthetic linker of five glycines replaced the IC domain. Each α4 or β2 TM domain contains 137 residues with an approximate molecular weight of 15 kDa. Glutamate mutations at the N- and C-termini, designed to lower the pI, were necessary to secure protein stability for NMR measurements. Mutation of three hydrophobic residues to serine within the TM2-TM3 linker of α4 or β2 was also instrumental to prevent protein destabilization. Direct exposure of hydrophobic residues to the aqueous phase in the absence of the EC domain resulted in protein precipitation in a short time period. Amino acid sequences showing mutations of the α4 and β2 TM domains are provided in the Supplementary Material (Fig. S1). The expressed proteins were purified by Ni-NTA (GE Healthcare) chromatography before and after overnight cleavage of the his-tagged region at 4 ºC. The purification buffer contained 50 mM Tris, 150 mM NaCl, and 0.5% LDAO, and proteins were eluted with imidazole. Each NMR sample had 0.25–0.3 mM protein, 1–2% (40–80 mM) LDAO, 5 mM phosphate acetate pH 4.7, 10 mM NaCl, and 20 mM 2-mercaptoethanol to prevent disulfide bond formation. 5% D_2O was added to the NMR samples for deuterium lock in NMR measurements. In terms of the α4 and β2 contents, we prepared four types of samples: (1) pure α4; (2) pure β2; (3) α4:β2=2:3; and (4) α4:β2=3:2.

2.2 NMR spectroscopy

NMR spectra were acquired at 45 ºC on Bruker Avance 600, 700, 800, and 900 MHz spectrometers equipped with a triple-resonance inverse-detection cryoprobe, TCI (Bruker Instruments, Billerica, MA). Spectral windows of 11 or 13 ppm (1024 data points) in the ^{1}H dimension and 22 or 24 ppm (128 data points) in ^{15}N dimension with a relaxation delay of 1 s (or 1.5 s at 900 MHz) were used for collecting ^{1}H-^{15}N TROSY-HSQC spectra. ^{1}H-^{13}C HSQC spectra were acquired as 1024 points in the ^{1}H dimension and 256 increments in the ^{13}C dimension with spectral windows of 11 ppm (^{1}H) and 64 ppm (^{13}C). For chemical shift assignment, we performed a suite of 3D experiments, including HNCA and HN(CO)CA (1024 × 36 × 80, 600 or 700 MHz) with a spectral window of 18 ppm in the ^{13}C dimension, HNCO (1024 × 36 × 40, 600 or 700 MHz) with a ^{13}C spectral width of 10 ppm, ^{15}N-edited NOESY (1024 × 36 × 160) with a mixing time of 120 ms at 900 MHz and 150 ms at 700 MHz, and ^{13}C-edited NOESY (1024 × 36 × 192, 700 MHz) with a mixing time of 150 ms. In addition, CBCA(CO)NH (1024 × 32 × 80, 700 MHz) with a ^{13}C spectral window of 60 ppm was acquired. In order to evaluate the temperature dependence of individual residue chemical shifts, α4 and β2 ^{1}H-^{15}N TROSY-HSQC spectra were collected at 40, 43, 45, and 48 ºC. The residues with temperature coefficients < 4.5 ppb/K were considered to have hydrogen binding [38]. The observed ^{1}H chemical shifts were referenced to the DSS resonance at 0 ppm and the ^{15}N and ^{13}C chemical shifts were indirectly referenced [39].

2.3 Size exclusion chromatography–multi-angle light scattering (SEC-MALS) analysis

The molar masses of the protein-detergent complexes were determined using size exclusion chromatography (Superdex 200 10/300, GE Healthcare) coupled with multi-angle light scattering (HELEOS, Wyatt Technology), UV (Agilent 1100 Series; Agilent Technology), and differential refractive index (Optilab rEX; Wyatt Technology) detection. The measurements were performed on the samples that had been used for NMR in 10 mM sodium acetate pH 4.6, 100 mM NaCl, 0.05% LDAO at a flow rate of 0.5 mL/min at room

temperature. HELEOS calibration constants were determined in the same buffer using chicken egg lysozyme (Affymetrix) as the standard. Light scattering data was analyzed and the molar mass of the protein-detergent complex was determined using ASTRA software (Wyatt Technology) [40]. The conjugate analysis module of ASTRA was used to differentiate contributions of the protein and detergent to the molecular weight of each complex. The specific refractive index (dn/dc) values of 0.185 and 0.148 were used for the protein and LDAO detergent, respectively [41]. The UV extinction coefficients of α4 and β2 were calculated from their sequences. A measured UV extinction coefficient of 0.06 for a 1% solution at 280 nm was used for LDAO.

2.4 The Na^+ flux assay for functional measurements

The Na^+ flux assay, as measured by the reduction of Sodium Green™ dye (Invitrogen, Carlsbad, CA) fluorescence due to Na^+ leaving the vesicles through open channels, is an effective way to macroscopically assess activity of the α4β2 TM channels. We prepared 25 mM vesicles with ~500 μM α4β2. The vesicles contained egg phosphatidylcholine (PC)/ phosphatidylglycerol (PG) in a 3:1 molar ratio and lipid biotinyl-cap-PE (1 mol %). Lipids dissolved in chloroform were mixed with α4β2 and dried to a thin film by nitrogen gas. Residual organic solvent was removed by vacuum overnight. The lipid-protein mixture was hydrated overnight at 42°C with a buffer solution containing 20 mM Tris, 100 mM NaCl, and 3 μM Sodium Green™ at pH 7.5. The vesicles were obtained by multiple subsequent cycles of freeze/thaw and sonication. Sodium Green™ dye outside the vesicles was removed by extensive dialysis.

The Na^+ flux assay was performed using an Olympus IX81 microscope (Olympus America, Center Valley, PA), equipped with a Sutter Lambda xenon exciter light source, various excitation and emission filters, and an ORCA-ER digital camera. For each measurement, vesicles containing α4β2 were added onto the streptavidin coated glass slide. The image acquisition started before vesicles were washed with a buffer solution (50mM CaCl2 20mM Tris at pH 7.5) to dilute the extra-vesicle Na^+ concentration. The resulting Na^+ concentration gradient drove Na^+ out of the vesicles when channels were formed. Consequently the fluorescence intensity resulting from Sodium Green™ trapped inside vesicles was reduced. Decay of the Sodium Green™ fluorescence intensity within each cluster of vesicles was recorded using the program In-vivo and analyzed by MetaMorph (Molecular Devices, Sunnyvale, CA).

2.5 Data processing, analysis and structure calculations

NMR data were processed using NMRPipe 4.1 and NMRDraw 1.8 [42], and analyzed using Sparky 3.10 [43]. ^{1}H, ^{15}N, and ^{13}C chemical shift assignments for the TM domains of the AChR α4 and β2 subunits were performed manually using the acquired NMR spectra. Initial NOE cross-peak assignment was carried out manually and then more cross-peaks were assigned using CYANA 2.1 [44]. For both the α4 and β2 subunits, a total of 100 monomer structures were calculated using CYANA 3.0 based on NOE and hydrogen-bonding restraints, as well as Talos dihedral angle restraints derived from the chemical shifts [45]. Restraints for α4 and β2 are shown in Tables S1 and S2, respectively. Of these 100 structures, 30 with the lowest target function underwent further refinement using Cyana 3.0. A final bundle of 20 structures with the lowest target function was analyzed using VMD [46] and Molmol [47]. Contact maps were used for evaluating tertiary structures of individual subunits and comparing tertiary structures of different proteins. Contact areas between residues were analyzed using the CMA component of the SPACE suite [48]. Contact surface area was defined as the area between two atoms into which a solvent molecule cannot fit.

The α4 and β2 structures with the smallest RMSDs from their respective average structures were used for building pentameric models. The MATLAB® programming environment was used to input structure coordinates, perform coordinate transformations, and save a pentamer model in PDB format. Individual structures of α4 and β2 were first oriented such that each helical axis of TM2 was parallel to the *Z*-axis. The helical axis of TM2 was determined using only the backbone atoms of residues from 245 to 266 for α4 or 239 to 260 for β2. The structures were then duplicated to form $(\alpha4)_2(\beta2)_3$ and $(\alpha4)_3(\beta2)_2$ pentamers, where the center of the backbone atoms for each of the five TM2 helices was located on the vertices of a five-fold symmetric pentagon. Orientations of the α4 and β2 subunits were adjusted to satisfy the NMR chemical shift perturbation data, in which interacting residues between α4 and β2 were indicated. The pore lining residues (T248, S252, and V259) for the α4 subunit were also set to be consistent with experimental results from the substituted cysteine accessibility method [49]. We constructed two pentameric models of α4β2 with 2:3 and 3:2 ratios for α4 to β2. It is plausible that α4β2 in our sample preparation was in both stoichiometries [50, 51]. The pentameric structural models were subjected to 2000 steps of steepest descent minimization in NAMD 2.6 [52] with a 100 kcal/mol restraint on backbone atoms. The pore radius profiles were obtained using the HOLE program [53] with a step size of 0.2 Å along the pore axis.

3. Results and Discussion

3.1 Structures of the TM domains of the α4 and β2 nAChR subtypes

Fig. 1 shows representative NMR spectra of the α4 and β2 TM domains in the LDAO micelles. Well-resolved peaks in the spectra for individual residues and sustained protein stability were achieved only after intensively tweaking sample conditions. In addition to mutating a few residues in the terminal and loop regions and choosing a proper detergent, setting a proper molar ratio of detergent to protein (D:P) is also critical for the quality of NMR spectra. We found that the D:P affected the oligomeric state of α4 or β2. When the D:P was lower than 100, the number of resonance peaks in the α4 or β2 NMR spectra decreased substantially (Fig. S2), indicating the formation of large size aggregates. When the D:P was greater than 300, quality of the NMR spectra worsened after a short time period, presumably due to an unfavorable oligomeric state for α4 or β2. An optimal condition for protein stability and NMR spectral quality is to have the D:P in the range of 200 – 250. This condition has been used for acquiring data reported here. The oligomeric state of α4 or β2 under this condition was determined using size exclusion chromatography coupled with multi-angle light scattering (SEC-MALS). The average molar mass of the α4 or β2 assemblies was obtained by differentiating the contributions of protein and detergent to the molar mass of each complex using the differential dn/dc and UV extinction coefficients for the protein and detergent (Fig. S3). The SEC-MALS data showed that the TM domains of α4 or β2 formed homo-pentamers with an average molar mass of 74.5 kDa and 75.2 kDa, respectively.

Structures of the TM domains for subunits α4 and β2 (Fig. 2) were determined based on constraints generated from NMR experiments. Details of constraints for distances, dihedral angles, hydrogen bonding and statistics of the structural calculations are provided in the supplemental materials (Fig. S4, Table S1, and Table S2). For each subunit type, there are obvious structural characteristics of four helices. Sufficient long-range NOE restraints between different TM helices were identified for generating tertiary folding (Fig. S5). The backbone RMSD of the helical regions among the 20 lowest energy structures for α4 or β2 is less than 1 A. Because of their high sequence homology (~88%), the α4 and β2 TM domains share considerable structure similarity (Fig. 2C), and the backbone RMSD of their helical regions is ~1.5 A. Variations of helical arrangement between α4 and β2 are small, as reflected in similar patterns of residue contact maps of the two subunits (Fig. S6).

To evaluate how a membrane mimetic environment affects folding of the TM domains, we compared the β2 structure solved in LDAO micelles (Fig. 2) with our β2 structure (PDB ID: 2KSR) determined previously in the HFIP-water mixture [9]. Interestingly, the two β2 structures resembled each other, as shown in the superimposed structures and the overlapped contact maps in Fig. S7. The result suggests that helix-helix packing forces dominate assembly of the β2 TM domain. A notable difference between two ensembles of the β2 structures is the bending of the TM2 helix near the TM2-TM3 linker, which was observed in the HFIP/water mixtures but not in LDAO. Such a conformational difference may reflect differences in mimicking the water/membrane interface between the HFIP-water mixtures and the LDAO micelles.

We also compared the α4 and β2 NMR structures with the structures of GLIC, GluCl, and the α1 and β1 *Torpedo* nAChR (Fig. S6, Fig. S7). The helical length of the pore-lining TM2 in α4 and β2 resembles that in the GLIC and GluCl structures [13, 14, 16], but is shorter than that in the *Torpedo* nAChR structural model [12]. The c-terminus of the TM2 helix in α4, β2, GLIC and GluCl ends a few residues before the conserved proline in the TM2-TM3 linker. The same helical termination at the c-terminus of TM2 was also found previously in different membrane mimetic environments [9, 54]. However, in the *Torpedo* nAChR structural mode, the TM2 helix ends three residues after this conserved proline. Another interesting observation is on the TM3-TM4 linkers of these proteins. Only two or six residues link TM3 and TM4 in GLIC or GluCl, respectively. On the other hand, the TM3-TM4 linker in the *Torpedo* or the α4β2 nAChR is a large intracellular domain that often involves over a hundred residues. The TM3-TM4 linker in the *Torpedo* nAChR shows a helical segment [12]. To have the protein size manageable for NMR, we removed the majority of the intracellular domain and kept only 18 residues (13 original loop residues and an additional five consecutive glycine residues) for the TM3-TM4 linker in α4 and β2. The drastic variations in the number of the TM3-TM4 linker residues among these proteins do not profoundly alter the four helical bundle motifs of the TM domains, as shown in Fig. S6 and Fig. S7. The structural resilience to modification of the intracellular region is in accord with observations that the $GABA_A$ and $5HT_3$ receptors were functional after the deletion of their intracellular domains [23].

3.2 Pentameric structure model of the α4β2 TM domain

To determine whether the TM domains of α4 and β2 interact with each other and their oligomerization state in LDAO micelles, we performed NMR and SEC-MALS measurements on mixtures of α4 and β2.

To obtain a better resolution, only one subunit type in the α4β2 mixture was ^{15}N - or ^{13}C-labeled for each NMR spectrum. In other words, only one set of residues, either from α4 or β2 in the mixture, was observed in a NMR spectrum. If there were no interactions between α4 and β2, the NMR spectrum of the mixture would be the same as the spectrum of α4 or β2 alone. On the other hand, differences between the NMR spectra of a single subunit type and the α4β2 mixture are indicative of interactions between two different subunits. As shown in the spectral overlay of α4 and the α4β2 mixture in Fig. 3A, several residues of the α4 subunit were perturbed by the addition of the unlabeled β2. Similarly, β2 was perturbed in the NMR spectra when it was mixed with the unlabeled α4. Fully annotated spectra for α4 in the presence of β2 or β2 in the presence of α4 are provided in the supplementary materials (Figs. S8 and S9). These NMR data suggested that the α4 and β2 TM domains interacted with each other and formed oligomers in LDAO micelles. The oligomeric state of the α4 and β2 TM domains in the NMR samples was determined using size exclusion chromatography coupled with SEC-MALS. As shown in Fig. 3B, the average molar mass of the α4β2 oligomers across the elution peak is 74.6 kD, which is virtually the same as the expected molar mass of 75 kD for a pentamer of the α4 and β2 TM domains. The TM domain of α4 or

β2 alone also formed homo-pentamers (Fig. S3), though the intact α4 or β2 subunits have not been found to form homo-pentamers. These results suggest that without the extracellular domain the TM domain is sufficient for spontaneous pentameric assemblies in a membrane mimetic environment.

Changes in the α4 and β2 NMR spectra due to a perturbation from their interacting partners are relatively small and limited to only a few residues (Fig. 3A, Figs. S8 and S9). This is understandable for at least two reasons. First, the pure or mixed subunits are in the same oligomeric state. Second, the α4 and β2 TM domains contain a high percentage of identical residues. Because of these reasons, when the adjacent subunit was changed from the same type to a different type in the pentameric assemblies, the structure of the α4 or β2 subunit did not change considerably. Thus, we built the α4β2 pentameric models using the NMR subunit structures (Fig. 2). The NMR chemical shift perturbation data (Figs. S8 and S9) were used to guide spatial arrangement of interacting residues between α4 and β2 for building the model. For example, α4-L239 in the TM1 helix and β2-L294 in the TM3 helix were both affected by the presence of the complementary subunit in the chemical shift perturbation experiments. They are likely close to each other in space. Similar inter-subunit pairs were identified at different locations along the membrane normal (Fig. S10). They were used for assembling pentameric models.

The α4β2 nAChR was originally found to exist in the $(\alpha4)_2(\beta2)_3$ stoichiometry [55, 56], but later was also found to form $(\alpha4)_3(\beta2)_2$ [50, 51]. Thus, we constructed two models for both stoichiometries (Fig. 4). The pore lining residues, T2', S6', L9', V13', L17', and α4-E20' or β2-K20', agree with those determined previously using the substituted cysteine accessibility method (SCAM) [49, 57]. The pore radius profiles in Fig. 5 show funnel shaped channels for $(\alpha4)_2(\beta2)_3$ and $(\alpha4)_3(\beta2)_2$, opening widely at the extracellular end and narrowing gradually toward the intracellular end. The funnel shaped pore profile with a widely opened extracellular end was also observed in the GLIC and GluCl structures, where both channels were concluded as open channels [13, 14, 16]. The $(\alpha4)_2(\beta2)_3$ model is in an apparent open-channel conformation and its minimal pore radius at T2' (2.9 A) is greater than that in GLIC (~2.5 A). Although pore profiles resulting from backbones are nearly the same for both models, the pore radius at L9' is smaller in the $(\alpha4)_3(\beta2)_2$ model. The sidechain of L9' in α4 was protruded to the pore lumen slightly more than that in β2.

The α4β2 nAChR structural model analyses indicate that hydrophobic contact is the driving force to assemble the TM domains into a pentamer (Fig. S11). Leucine-isoleucine contacts (39%) and leucine-leucine contacts (31%) are the major residue contacts between two subunits. Other hydrophobic residues, including valine and methionine, contribute 22% to the inter-subunit residue contacts. There is only one pair of aromatic contacts (F298 -Y232) between α4 and β2 subunits. The importance of hydrophobic residues in the pentameric assembly was also demonstrated in a recent NMR study on phospholamban [58]. The interlocking of alternating leucine and isoleucine residues forms a leucine/isoleucine zipper to hold the phospholamban protomers [58].

The α4β2 nAChR structural models allow us to visualize findings implicated in previous experiments. Changing the stoichiometry of α4 and β2 altered Ca^{2+} permeability in α4β2 nAChR. Increasing the proportion of negative charges in $(\alpha4)_3(\beta2)_2$ was found to associate with increasing permeability to Ca^{2+} [59]. Indeed, as shown in Fig. 4, positively charged β2-K20' and negatively charged α4-E20' are located at the extracelluar pore entrance. A larger proportion of α4-E20' in $(\alpha4)_3(\beta2)_2$ provides a benefit by attracting Ca^{2+} to the pore entrance. Electrostatic interaction between β2-K20' and α4-E20' may also help to stabilize pentameric assemblies [60]. Results from previous photoaffinity labeling experiments on the α4β2 nAChR are well presented in, and explained by, our structural models. [^{125}I]TID, a

hydrophobic probe [61], was photolabeled onto the α4β2 nAChR for mapping the protein/lipid interface [62]. We highlighted the residues labeled by [^{125}I]TID in our α4β2 models (Fig. S12), including homologous residues α4-C582 and β2-C445 in TM4, α4-C226 and α4-C231 in TM1, and β2-C220 that is homologous to α4-C226 [62]. Clearly, our structures show exposure of α4-C582 and β2-C445 in TM4 and α4-C231 in TM1 to lipids. More interestingly, our structures show that α4-C582 and β2-C445 of TM4 face to α4-C226 and β2-C220 of TM1, respectively. They form a [^{125}I]TID binding pocket along with surrounding lipids. Although α4-C226 and β2-C220 are less exposed to lipids, their labeling by [^{125}I]TID could be facilitated by α4-C582 and β2-C445 in the same pockets. However, if the *Torpedo* nAChR model [12] is used for explaining the photolabeling data, α4-C582 and β2-C445 seem to have no association with α4-C226 and β2-C220, respectively (Fig. S12).

3.3 Functional Measurements of the α4β2 Assembly

NMR chemical shift perturbation experiments in combination with the SEC-MALS analysis provided evidence for the formation of the α4β2 pentameric assembly. In order to assess whether the α4β2 TM domains formed channels, we reconstituted α4 and β2 into lipid vesicles and performed the Na^+ flux assay. Significant reduction of Sodium Green™ dye fluorescence was observed in vesicles immediately after dilution of the extra-vesicle salt concentration only if the vesicles contained the α4β2 assembly (Fig. 6A). During the same measurement time, however, fluorescence remained almost the same in vesicles lacking α4β2 (Fig. 6B), confirming that the observed fluorescence reduction in Fig. 6A was not due to fluorescence bleaching. Efflux of Na^+ from the α4β2 containing vesicles is a compelling indication that the α4β2 TM domains are capable of forming channels transporting Na^+ across a membrane. The data in Fig. 6 suggest that the open conformation of the α4β2 assembly is thermodynamically accessible at room temperature, though it cannot tell how rapidly the closed and open conformations exchange spontaneously.

4. Conclusions

The study has delivered several novel findings. First, the atomic structures of the whole TM domains of the α4 and β2 nAChR subunits are solved for the first time in micelles by using NMR. These structures are valuable for understanding the biological and pharmacological properties of the α4β2 nAChR, particularly for characterizing mechanisms of action for existing drugs and indentifying plausible binding sites for new drugs. The methodology reported here for achieving high quality NMR spectra of transmembrane proteins is also useful for structural studies of other membrane proteins. Second, our SEC-MALS data provided compelling evidence for a pentameric oligomerization state of the TM domains of α4 and β2 as well as their mixtures under the NMR sample condition. The NMR results showed that hydrophobic interaction was the primary driving force for oligomerization of individual subunits. Third, the TM domains of α4 and β2 formed not merely pentameric assemblies. They are ion channels permeable to Na^+. Collectively, the study provides structural insight into the TM domains of the α4β2 nAChR. It offers a valuable structural framework for rationalizing extensive biochemical data collected previously on the α4β2 nAChR and for designing new therapeutic modulators.

Supplementary Material

Refer to Web version on PubMed Central for supplementary material.

Acknowledgments

We thank Ms. Sandra C. Hirsch for her editorial assistance. This work was supported by grants from the National Institute of Health (R01GM56257 and R01GM66358 to P.T. and R37GM049202 to Y.X.).

References

1. Evers AS, Steinbach JH. Supersensitive sites in the central nervous system. Anesthetics block brain nicotinic receptors. Anesthesiology. 1997; 86:760–762. [PubMed: 9105218]
2. Meyer PM, Strecker K, Kendziorra K, Becker G, Hesse S, Woelpl D, Hensel A, Patt M, Sorger D, Wegner F, Lobsien D, Barthel H, Brust P, Gertz HJ, Sabri O, Schwarz J. Reduced alpha4beta2*-nicotinic acetylcholine receptor binding and its relationship to mild cognitive and depressive symptoms in Parkinson disease. Arch Gen Psychiatry. 2009; 66:866–877. [PubMed: 19652126]
3. Lamb PW, Melton MA, Yakel JL. Inhibition of neuronal nicotinic acetylcholine receptor channels expressed in Xenopus oocytes by beta-amyloid1-42 peptide. J Mol Neurosci. 2005; 27:13–21. [PubMed: 16055943]
4. Picciotto MR, Zoli M, Rimondini R, Lena C, Marubio LM, Pich EM, Fuxe K, Changeux JP. Acetylcholine receptors containing the beta2 subunit are involved in the reinforcing properties of nicotine. Nature. 1998; 391:173–177. [PubMed: 9428762]
5. Le Foll B, Chefer SI, Kimes AS, Shumway D, Stein EA, Mukhin AG, Goldberg SR. Baseline expression of alpha4beta2* nicotinic acetylcholine receptors predicts motivation to self-administer nicotine. Biol Psychiatry. 2009; 65:714–716. [PubMed: 19095220]
6. Mori T, Zhao X, Zuo Y, Aistrup GL, Nishikawa K, Marszalec W, Yeh JZ, Narahashi T. Modulation of neuronal nicotinic acetylcholine receptors by halothane in rat cortical neurons. Mol Pharmacol. 2001; 59:732–743. [PubMed: 11259617]
7. Yamashita M, Mori T, Nagata K, Yeh JZ, Narahashi T. Isoflurane modulation of neuronal nicotinic acetylcholine receptors expressed in human embryonic kidney cells. Anesthesiology. 2005; 102:76–84. [PubMed: 15618790]
8. Flood P, Ramirez-Latorre J, Role L. Alpha 4 beta 2 neuronal nicotinic acetylcholine receptors in the central nervous system are inhibited by isoflurane and propofol, but alpha 7-type nicotinic acetylcholine receptors are unaffected. Anesthesiology. 1997; 86:859–865. [PubMed: 9105230]
9. Bondarenko V, Tillman T, Xu Y, Tang P. NMR structure of the transmembrane domain of the n-acetylcholine receptor beta2 subunit. Biochim Biophys Acta. 2010; 1798:1608–1614. [PubMed: 20441771]
10. Hamouda AK, Jin X, Sanghvi M, Srivastava S, Pandhare A, Duddempudi PK, Steinbach JH, Blanton MP. Photoaffinity labeling the agonist binding domain of alpha4beta4 and alpha4beta2 neuronal nicotinic acetylcholine receptors with [(125)I]epibatidine and 5[(125)I]A-85380. Biochim Biophys Acta. 2009; 1788:1987–1995. [PubMed: 19545536]
11. daCosta CJ, Michel Sturgeon R, Hamouda AK, Blanton MP, Baenziger JE. Structural characterization and agonist binding to human alpha4beta2 nicotinic receptors. Biochem Biophys Res Commun. 2011; 407:456–460. [PubMed: 21396349]
12. Unwin N. Refined structure of the nicotinic acetylcholine receptor at 4A resolution. J Mol Biol. 2005; 346:967–989. [PubMed: 15701510]
13. Bocquet N, Nury H, Baaden M, Le Poupon C, Changeux JP, Delarue M, Corringer PJ. X-ray structure of a pentameric ligand-gated ion channel in an apparently open conformation. Nature. 2009; 457:111–114. [PubMed: 18987633]
14. Hilf RJ, Dutzler R. Structure of a potentially open state of a proton-activated pentameric ligand-gated ion channel. Nature. 2009; 457:115–118. [PubMed: 18987630]
15. Hilf RJ, Dutzler R. X-ray structure of a prokaryotic pentameric ligand-gated ion channel. Nature. 2008; 452:375–379. [PubMed: 18322461]
16. Hibbs RE, Gouaux E. Principles of activation and permeation in an anion-selective Cys-loop receptor. Nature. 2011; 474:54–60. [PubMed: 21572436]
17. Brejc K, van Dijk WJ, Klaassen RV, Schuurmans M, van Der Oost J, Smit AB, Sixma TK. Crystal structure of an ACh-binding protein reveals the ligand-binding domain of nicotinic receptors. Nature. 2001; 411:269–276. [PubMed: 11357122]
18. Celie PH, van Rossum-Fikkert SE, van Dijk WJ, Brejc K, Smit AB, Sixma TK. Nicotine and carbamylcholine binding to nicotinic acetylcholine receptors as studied in AChBP crystal structures. Neuron. 2004; 41:907–914. [PubMed: 15046723]

19. Hansen SB, Sulzenbacher G, Huxford T, Marchot P, Taylor P, Bourne Y. Structures of Aplysia AChBP complexes with nicotinic agonists and antagonists reveal distinctive binding interfaces and conformations. EMBO J. 2005; 24:3635–3646. [PubMed: 16193063]
20. Dellisanti CD, Yao Y, Stroud JC, Wang ZZ, Chen L. Crystal structure of the extracellular domain of nAChR alpha1 bound to alpha-bungarotoxin at 1.94 A resolution. Nat Neurosci. 2007; 10:953–962. [PubMed: 17643119]
21. Li SX, Huang S, Bren N, Noridomi K, Dellisanti CD, Sine SM, Chen L. Ligand-binding domain of an alpha(7)-nicotinic receptor chimera and its complex with agonist. Nat Neurosci. 2011; 14:1253–1259. [PubMed: 21909087]
22. Fenster CP, Beckman ML, Parker JC, Sheffield EB, Whitworth TL, Quick MW, Lester RA. Regulation of alpha4beta2 nicotinic receptor desensitization by calcium and protein kinase C. Mol Pharmacol. 1999; 55:432–443. [PubMed: 10051526]
23. Jansen M, Bali M, Akabas MH. Modular design of Cys-loop ligand-gated ion channels: functional 5-HT3 and GABA rho1 receptors lacking the large cytoplasmic M3M4 loop. J Gen Physiol. 2008; 131:137–146. [PubMed: 18227272]
24. Jensen AA, Frolund B, Liljefors T, Krogsgaard-Larsen P. Neuronal nicotinic acetylcholine receptors: structural revelations, target identifications, and therapeutic inspirations. J Med Chem. 2005; 48:4705–4745. [PubMed: 16033252]
25. Jozwiak K, Ravichandran S, Collins JR, Wainer IW. Interaction of noncompetitive inhibitors with an immobilized alpha3beta4 nicotinic acetylcholine receptor investigated by affinity chromatography, quantitative-structure activity relationship analysis, and molecular docking. J Med Chem. 2004; 47:4008–4021. [PubMed: 15267239]
26. Wilson GG, Karlin A. The location of the gate in the acetylcholine receptor channel. Neuron. 1998; 20:1269–1281. [PubMed: 9655513]
27. Arias HR, Rosenberg A, Targowska-Duda KM, Feuerbach D, Jozwiak K, Moaddel R, Wainer IW. Tricyclic antidepressants and mecamylamine bind to different sites in the human alpha4beta2 nicotinic receptor ion channel. Int J Biochem Cell Biol. 2010; 42:1007–1018. [PubMed: 20223294]
28. Pandya A, Yakel JL. Allosteric modulators of the alpha4beta2 subtype of neuronal nicotinic acetylcholine receptors. Biochem Pharmacol. 2011; 82:952–958. [PubMed: 21596025]
29. Weltzin MM, Schulte MK. Pharmacological characterization of the allosteric modulator desformylflustrabromine and its interaction with alpha4beta2 neuronal nicotinic acetylcholine receptor orthosteric ligands. J Pharmacol Exp Ther. 2010; 334:917–926. [PubMed: 20516140]
30. Nirthanan S, Garcia G 3rd, Chiara DC, Husain SS, Cohen JB. Identification of binding sites in the nicotinic acetylcholine receptor for TDBzl-etomidate, a photoreactive positive allosteric effector. J Biol Chem. 2008; 283:22051–22062. [PubMed: 18524766]
31. Chiara DC, Dangott LJ, Eckenhoff RG, Cohen JB. Identification of nicotinic acetylcholine receptor amino acids photolabeled by the volatile anesthetic halothane. Biochemistry. 2003; 42:13457–13467. [PubMed: 14621991]
32. Liu LT, Willenbring D, Xu Y, Tang P. General anesthetic binding to neuronal alpha4beta2 nicotinic acetylcholine receptor and its effects on global dynamics. J Phys Chem B. 2009; 113:12581–12589. [PubMed: 19697903]
33. Liu LT, Haddadian EJ, Willenbring D, Xu Y, Tang P. Higher susceptibility to halothane modulation in open- than in closed-channel alpha4beta2 nAChR revealed by molecular dynamics simulations. J Phys Chem B. 2010; 114:626–632. [PubMed: 20014754]
34. Mowrey D, Haddadian EJ, Liu LT, Willenbring D, Xu Y, Tang P. Unresponsive correlated motion in alpha7 nAChR to halothane binding explains its functional insensitivity to volatile anesthetics. J Phys Chem B. 2010; 114:7649–7655. [PubMed: 20465243]
35. Cui T, Canlas CG, Xu Y, Tang P. Anesthetic effects on the structure and dynamics of the second transmembrane domains of nAChR alpha4beta2. Biochim Biophys Acta. 2010; 1798:161–166. [PubMed: 19715664]
36. Opella SJ, Marassi FM, Gesell JJ, Valente AP, Kim Y, Oblatt-Montal M, Montal M. Structures of the M2 channel-lining segments from nicotinic acetylcholine and NMDA receptors by NMR spectroscopy. Nat Struct Biol. 1999; 6:374–379. [PubMed: 10201407]

37. Marley J, Lu M, Bracken C. A method for efficient isotopic labeling of recombinant proteins. J Biomol NMR. 2001; 20:71–75. [PubMed: 11430757]
38. Baxter NJ, Williamson MP. Temperature dependence of 1H chemical shifts in proteins. J Biomol NMR. 1997; 9:359–369. [PubMed: 9255942]
39. Wishart DS, Bigam CG, Yao J, Abildgaard F, Dyson HJ, Oldfield E, Markley JL, Sykes BD. 1H, 13C and 15N chemical shift referencing in biomolecular NMR. J Biomol NMR. 1995; 6:135–140. [PubMed: 8589602]
40. Folta-Stogniew E, Williams KR. Determination of molecular masses of proteins in solution: Implementation of an HPLC size exclusion chromatography and laser light scattering service in a core laboratory. J Biomol Tech. 1999; 10:51–63. [PubMed: 19499008]
41. Strop P, Brunger AT. Refractive index-based determination of detergent concentration and its application to the study of membrane proteins. Protein Sci. 2005; 14:2207–2211. [PubMed: 16046633]
42. Delaglio F, Grzesiek S, Vuister GW, Zhu G, Pfeifer J, Bax A. NMRPipe: a multidimensional spectral processing system based on UNIX pipes. J Biomol NMR. 1995; 6:277–293. [PubMed: 8520220]
43. Goddard, TD.; Kneller, DG. SPARKY 3. University of California; San Francisco: 2001.
44. Guntert P, Mumenthaler C, Wuthrich K. Torsion angle dynamics for NMR structure calculation with the new program DYANA. J Mol Biol. 1997; 273:283–298. [PubMed: 9367762]
45. Cornilescu G, Delaglio F, Bax A. Protein backbone angle restraints from searching a database for chemical shift and sequence homology. J Biomol NMR. 1999; 13:289–302. [PubMed: 10212987]
46. Humphrey W, Dalke A, Schulten K. VMD: visual molecular dynamics. J Mol Graph. 1996; 14:33–38. 27–38. [PubMed: 8744570]
47. Koradi R, Billeter M, Wuthrich K. MOLMOL: a program for display and analysis of macromolecular structures. J Mol Graph. 1996; 14:51–55. 29–32. [PubMed: 8744573]
48. Sobolev V, Eyal E, Gerzon S, Potapov V, Babor M, Prilusky J, Edelman M. SPACE: a suite of tools for protein structure prediction and analysis based on complementarity and environment. Nucleic Acids Res. 2005; 33:W39–43. [PubMed: 15980496]
49. Quek GXJ, Lin D, Halliday JI, Absalom N, Ambrus JI, Thompson AJ, Lochner M, Lummis SCR, McLeod MD, Chebib M. Identifying the Binding Site of Novel Methyllycaconitine (MLA) Analogs at alpha 4 beta 2 Nicotinic Acetylcholine Receptors. Acs Chemical Neuroscience. 2010; 1:796–809.
50. Zwart R, Vijverberg HP. Four pharmacologically distinct subtypes of alpha4beta2 nicotinic acetylcholine receptor expressed in Xenopus laevis oocytes. Mol Pharmacol. 1998; 54:1124–1131. [PubMed: 9855643]
51. Nelson ME, Kuryatov A, Choi CH, Zhou Y, Lindstrom J. Alternate stoichiometries of alpha4beta2 nicotinic acetylcholine receptors. Mol Pharmacol. 2003; 63:332–341. [PubMed: 12527804]
52. Phillips JC, Braun R, Wang W, Gumbart J, Tajkhorshid E, Villa E, Chipot C, Skeel RD, Kale L, Schulten K. Scalable molecular dynamics with NAMD. J Comput Chem. 2005; 26:1781–1802. [PubMed: 16222654]
53. Smart OS, Neduvelil JG, Wang X, Wallace BA, Sansom MS. HOLE: a program for the analysis of the pore dimensions of ion channel structural models. J Mol Graph. 1996; 14:354–360. 376. [PubMed: 9195488]
54. Bondarenko V, Yushmanov VE, Xu Y, Tang P. NMR study of general anesthetic interaction with nAChR beta2 subunit. Biophys J. 2008; 94:1681–1688. [PubMed: 17993502]
55. Anand R, Conroy WG, Schoepfer R, Whiting P, Lindstrom J. Neuronal nicotinic acetylcholine receptors expressed in Xenopus oocytes have a pentameric quaternary structure. J Biol Chem. 1991; 266:11192–11198. [PubMed: 2040627]
56. Cooper E, Couturier S, Ballivet M. Pentameric structure and subunit stoichiometry of a neuronal nicotinic acetylcholine receptor. Nature. 1991; 350:235–238. [PubMed: 2005979]
57. Akabas MH, Kaufmann C, Archdeacon P, Karlin A. Identification of acetylcholine receptor channel-lining residues in the entire M2 segment of the alpha subunit. Neuron. 1994; 13:919–927. [PubMed: 7524560]

58. Verardi R, Shi L, Traaseth NJ, Walsh N, Veglia G. Structural topology of phospholamban pentamer in lipid bilayers by a hybrid solution and solid-state NMR method. Proc Natl Acad Sci U S A. 2011; 108:9101–9106. [PubMed: 21576492]

59. Tapia L, Kuryatov A, Lindstrom J. Ca2+ permeability of the (alpha4)3(beta2)2 stoichiometry greatly exceeds that of (alpha4)2(beta2)3 human acetylcholine receptors. Mol Pharmacol. 2007; 71:769–776. [PubMed: 17132685]

60. Saladino AC, Xu Y, Tang P. Homology modeling and molecular dynamics simulations of transmembrane domain structure of human neuronal nicotinic acetylcholine receptor. Biophys J. 2005; 88:1009–1017. [PubMed: 15574706]

61. Blanton MP, Cohen JB. Mapping the lipid-exposed regions in the Torpedo californica nicotinic acetylcholine receptor. Biochemistry. 1992; 31:3738–3750. [PubMed: 1567828]

62. Hamouda AK, Sanghvi M, Chiara DC, Cohen JB, Blanton MP. Identifying the lipid-protein interface of the alpha4beta2 neuronal nicotinic acetylcholine receptor: hydrophobic photolabeling studies with 3-(trifluoromethyl)-3-(m-[125I]iodophenyl)diazirine. Biochemistry. 2007; 46:13837–13846. [PubMed: 17994769]

Highlights

- The structures of the α4β2 TM domains are solved for the first time in micelles.
- The α4β2 TM domains alone can form pentameric channels permeable to Na+.
- The reported methods are useful for structural studies of other membrane proteins.
- The study offers a framework for rationalizing previous data collected on α4β2.
- The structures are valuable for designing new therapeutic modulators of nAChRs.

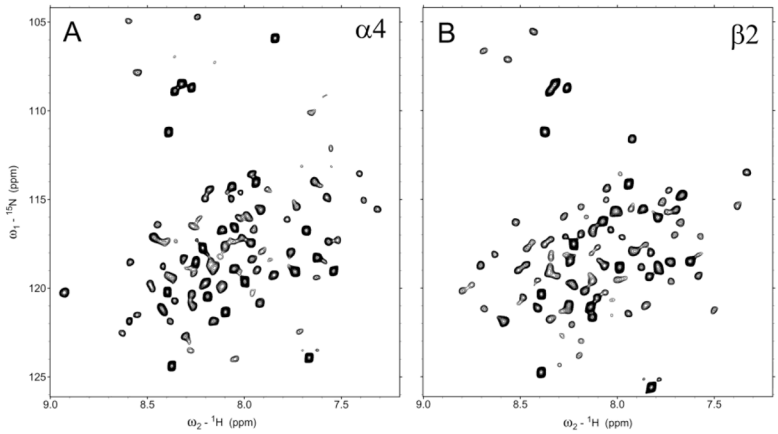

Fig. 1.

^{1}H-^{15}N TROSY-HSQC spectra of the transmembrane domain of the human n-acetylcholine receptor (**A**) α4 and (**B**) β2 subunits. The spectra were acquired with 0.25 mM α4 or β2 in 10 mM sodium acetate, 10 mM NaCl, and 60 mM LDAO at pH 4.7 and 45ºC. For clarity, the chemical shift assignment for each peak is omitted here but provided in the Supplementary Material.

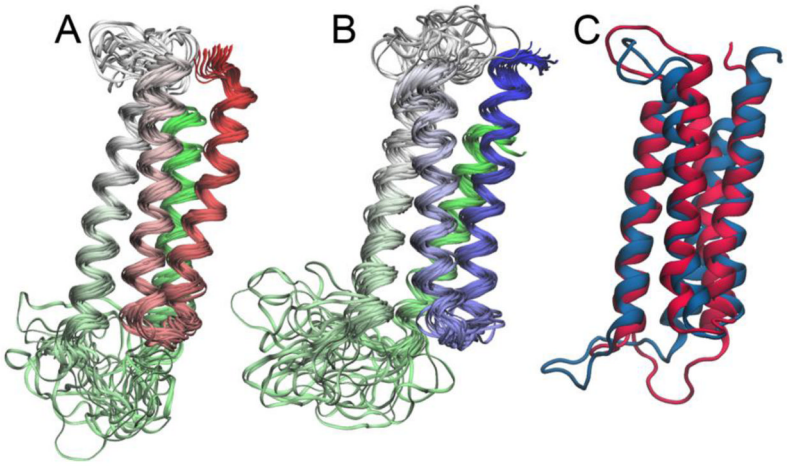

Fig. 2.

A bundle of the 20 lowest-energy NMR structures for (**A**) α4 and (**B**) β2. The color scheme varies gradually from red in (A) or blue in (B) for TM1 to green for TM4. (**C**) Overlay of the representative structures of α4 (red) with β2 (blue). Details of the NMR structural restraints and statistics for the refined structures are provided in Supplementary Materials.

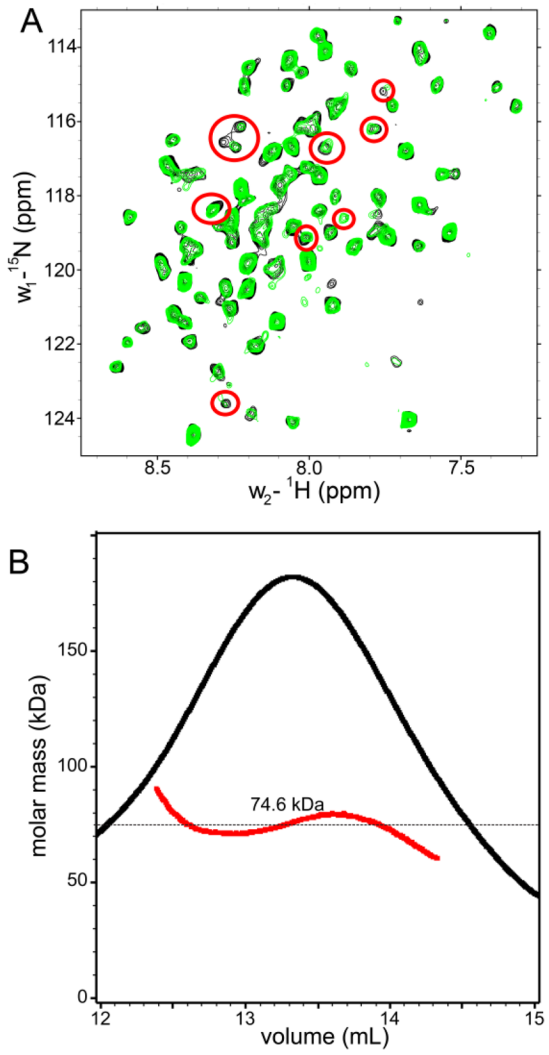

Fig. 3.

(**A)** Overlay of ^{1}H-^{15}N TROSY-HSQC spectra of α4 in the absence (black) and presence (green) of β2. Peaks circled in red showed changes in α4 chemical shift after the addition of β2, signifying interactions between α4 and β2. A limited number of residues experiencing changes in chemical shift suggested that the presence of β2 did not significantly alter the α4 structure. (**B)** Size exclusion chromatography–multi-angle light scattering analysis indicated the formation of the α4β2 pentameric assembly. The molar mass (red) of the α4β2 assembly in the nAChR α4β2-detergent complex was obtained using conjugate analysis and is shown across the elution peak (black) from size exclusion chromatography. The average molar mass of the α4β2 assembly is 74.6 kD. The dotted line indicates the expected molar mass of 75 kD.

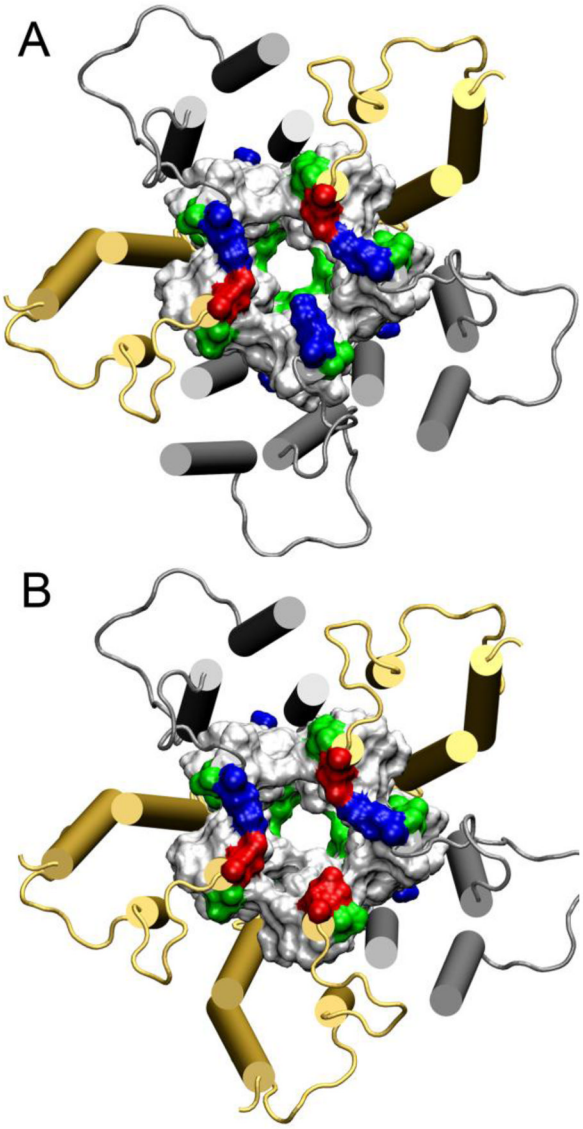

Fig. 4.

Top views of the α4β2 pentamer models: (**A**) $(\alpha4)_2(\beta2)_3$ and (**B**) $(\alpha4)_3(\beta2)_2$. Cartoon presentations for α4 and β2 subunits are colored orange and gray, respectively. Residues of TM2 are shown in surface and colored according to residue types, acidic in red, basic in blue, polar in green, and non-polar in white.

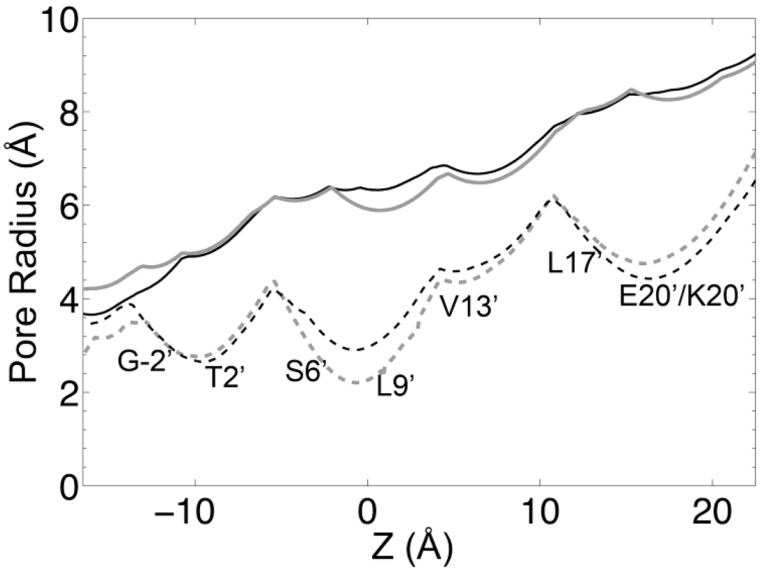

Fig. 5.

Pore-radius profiles for the $(\alpha 4)_2(\beta 2)_3$ (black) and $(\alpha 4)_3(\beta 2)_2$ (gray) models determined by the backbone atoms (solid line) or including the side chains (dashed line). Positions of the pore lining residues are highlighted. Pore profiles were generated using the HOLE program [53].

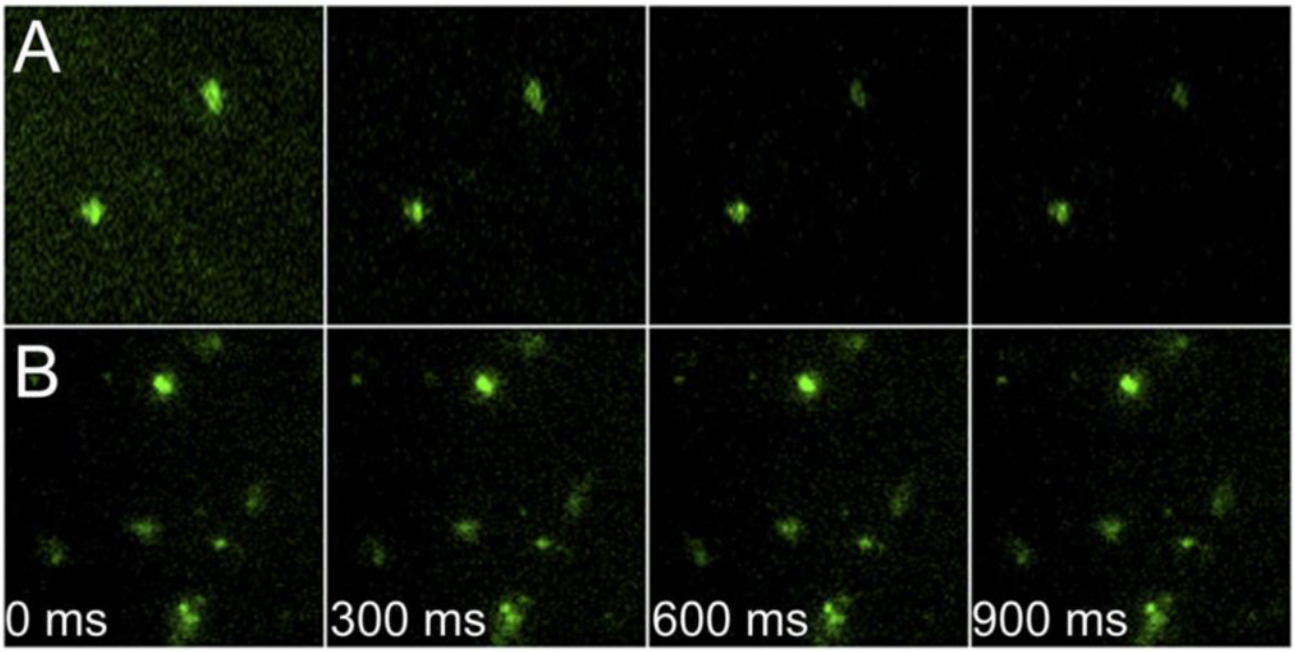

Fig. 6.

Fluorescence images of the Na^+ flux assay on vesicles in the (**A**) presence and (**B**) absence of the α4β2 nAChR channels at different time points. Membrane-impermeable Sodium Green fluorescent dyes were enclosed and trapped inside the vesicles to probe intra-vesicle Na^+ concentrations. The fluorescence intensity of the vesicles with α4β2 channels in (A) decreased significantly within a short period of time after washing away extra-vesicle sodium, indicating Na^+ efflux through the channels. However, fluorescence intensity of the control vesicles without α4β2 in (B) remained nearly constant before and after washing away extra-vesicle Na^+ during the same tine period.